Distinguishing a rotating Kiselev black hole from a naked singularity using the spin precession of a test gyroscope

Muhammad Rizwan,[1,*] Mubasher Jamil,[1,†] and Anzhong Wang[2,‡]

[1]*Department of Mathematics, School of Natural Sciences (SNS), National University of Sciences and Technology (NUST), H-12 Islamabad, Pakistan*

[2]*GCAP-CASPER, Physics Department, Baylor University, Waco, Texas 76798-7316, USA, and Institute for Advanced physics and Mathematics, Zhejiang University of Technology, Hangzhou 310032, China*

(Received 22 February 2018; published 9 July 2018)

We study the critical values of the quintessential and spin parameters, to distinguish a rotating Kiselev black hole from a naked singularity. For any value of the dimensionless quintessential parameter $\omega_q \in (-1, -1/3)$, when increasing the value of the quintessential parameter α, the size of the event horizon increases, whereas the size of the outer horizon decreases. We then study the spin precession of a test gyroscope attached to a stationary observer in this spacetime. Using the spin precessions we differentiate black holes from naked singularities. If the precession frequency becomes larger as an observer approaches the central object in the quintessential field along any direction, then the spacetime is a black hole. A spacetime will contain a naked singularity if the precession frequency remains finite everywhere except at the singularity itself. Finally, we study the Lense-Thirring precession frequency for a rotating Kiselev black hole and the geodetic precession for a Kiselev black hole.

DOI: 10.1103/PhysRevD.98.024015

I. INTRODUCTION

Current research on observational measurements predicts the accelerating expansion of the Universe, which is due to the presence of a state with negative pressure [1–3]. The negative pressure could be due to a cosmological constant or a so-called "dark energy" [4]. This energy is responsible for repulsive gravitational effects in the recent Universe and usually it is modeled as an exotic fluid. The fluid can be considered such that the state parameter ω is the ratio of the fluid pressure p to its density ρ, that is, $\omega = p/\rho$. The different dark energy models that have been proposed include quintessence [5,6], phantom dark energy [7,8], quintom [9,10], K essence [11], and others. The difference between these models of dark energy is the value of the parameter ω_q.

To study the dynamics of the recent Universe we have to consider repulsive gravitational effects caused by negative pressure due to the presence of dark energy. Quintessence is a candidate for dark energy, according to which the dimensionless quintessential state parameter ω_q is related to the pressure p and energy density ρ of the quintessential field through the equation of state of the quintessential field, $p = \omega_q \rho$ [5]. Furthermore, the range of the parameter ω_q is $-1 < \omega_q < -1/3$ [12–14]. If the quintessence matter exists throughout the Universe, it can also be around a black hole. A spherically symmetric static black hole in a quintessential matter field, which is a generalization of Schwarzschild and Schwarzschild–anti de Sitter (AdS) black holes, is known as a Kiselev black hole (KBH) [5]. A KBH and its charged version have been discussed in different ways. The thermodynamics and phase transition of a charged KBH were studied in Refs. [15–17]. The strong gravitational lensing by a KBH and a charged KBH were discussed in Refs. [18,19]. Recently, using Newman and Janis' technique [20] and its modification [21], the rotational generalization of a KBH was given in Ref. [22]. The Kerr-Newman-AdS black hole solution in a quintessential matter field was also obtained in Ref. [23].

Due to the rotation of the central object, spacetime exhibits effects of the Lense-Thirring (LT) precession, which causes the dragging of locally inertial frames along the rotating spacetime [24–26]. Due to these effects, gyroscopes attached to stationary observers in such a spacetime precess with certain frequencies. In the weak-field approximations the magnitude of the precession frequency is proportional to the spin parameter of the central object and decreases as the cube of the distance from the central object [25,26]. The gyroscope also precesses due to the spacetime curvature of the central object, and this type of precession is known as geodetic precession or de Sitter precession [27,28]. These two

*m.rizwan@sns.nust.edu.pk
†mjamil@sns.nust.edu.pk
‡anzhong_wang@baylor.edu

effects are predicted by Einstein's theory of general relativity. Gravity Probe B has been launched to test these aspects of general relativity and to measure the precession rate due to the LT and geodetic effects relative to the Copernican system or the fixed star HR8703 (known as IM Pegasi) of a test gyro due to the rotation of the Earth [29]. The geodetic precessions in a Schwarzschild black hole and a KBH were studied in Refs. [30–32]. The LT precessions in the strong gravitational fields of Kerr and Kerr-Taub-NUT black holes were discussed in Ref. [33].

The existence of naked singularities during the gravitational collapse of massive stars is a topic of great interest for researchers in the fields of gravitational theory and relativistic astrophysics. The key question is how one can differentiate whether the ultimate product in the life cycle of a compact object under self-gravitational collapse is a naked singularity or a black hole. Mathematically, a black hole is solution of the Einstein field equations. A stationary vacuum Kerr solution of the Einstein field equations is characterized by two parameters, namely, the mass M and angular momentum J of the central object. If the spin parameter a (angular momentum per unit mass) satisfies the condition $M \geq a$, the Kerr solution represents a black hole and the Kerr singularity is contained in the event horizon. However, if $M < a$ the event horizon disappears, representing a naked singularity. Recently, Chakraborty *et al.* [34,35] gave the criteria based on the spin precession frequency of a test gyroscope attached to both static and stationary observers to differentiate black holes from naked singularities. Using these criteria, the Kerr black hole and naked singularities were discussed.

The aim of the present paper is to differentiate rotating black holes in quintessential matter (rotating KBH) from a naked singularity. A stationary rotating Kiselev solution of Einstein's field equations is characterized by four parameters: the black hole mass M, the spin parameter a, the dimensionless quintessential parameter ω_q, and the quintessential parameter representing the intensity of the quintessence energy α. In this paper we will give the critical values of the spin parameter a_c and quintessential parameter α_c to differentiate a black hole from a naked singularity. Note that the case with $\omega_q = -2/3$ was already discussed [22]. We generalize the earlier work for general ω_q and study the critical values of the quintessential and spin parameters. Then, we perform our analysis using the criteria of the spin precession of a gyroscope in a rotating black hole in a quintessential matter field (RKBH). We also study the effects of quintessential energy on the LT precession frequency for an RKBH and the geodetic precession of a KBH.

The rest of the paper is organized as follows. In Sec. II the RKBHs are discussed and critical values of the quintessential and spin parameters are presented to differentiate black holes from naked singularities. At the end of Sec. II critical values of the quintessential parameter for a KBH are given. The spin precession of a test gyroscope in an RKBH is discussed in Sec. III, form which we obtain the LT precession of a gyroscope in an RKBH and geodetic precession in a KBH. In Sec. IV, using the key observations of the spin precessions of test gyroscopes attached to stationary observers in an RKBH, we differentiate black holes from naked singularities. Section V is devoted to some concluding remarks.

II. ROTATING KISELEV BLACK HOLES

The line element of a rotating Kiselev black hole can be written as [22]

$$\begin{aligned} ds^2 = &-\left(1-\frac{2Mr+\alpha r^{1-3\omega_q}}{\Sigma}\right)dt^2+\frac{\Sigma}{\Delta}dr^2 \\ &-2a\sin^2\theta\left(\frac{2Mr+\alpha r^{1-3\omega_q}}{\Sigma}\right)d\phi dt+\Sigma d\theta^2 \\ &+\sin^2\theta\left[r^2+a^2+a^2\sin^2\theta\left(\frac{2Mr+\alpha r^{1-3\omega_q}}{\Sigma}\right)\right]d\phi^2, \end{aligned} \tag{1}$$

where

$$\Delta = r^2 - 2Mr + a^2 - \alpha r^{1-3\omega_q}, \qquad \Sigma = r^2 + a^2\cos^2\theta.$$

The associated stress-energy tensor of the quintessential field takes the form found in Ref. [22] with the quantities $(\epsilon, p_r, p_\theta, p_\phi)$ being given by

$$\begin{aligned} \epsilon = -p_r &= \frac{\alpha(1-3\omega_q)r^{2-3\omega_q}}{8\pi\Sigma^2}, \\ p_\theta = p_\phi &= \frac{\alpha(-1+3\omega_q)[2r^2+(2-3\omega_q)\Sigma]}{16\pi\Sigma^2}. \end{aligned} \tag{2}$$

It should be noted that here M does not represent the total mass (or total energy) of the spacetime. By evaluating the Komar integrals, we will get the total mass M_T interior to the surface $r = r_0$, and the corresponding total angular momentum J_T of the RKBH, which are related to the mass M and angular momentum J of the Kerr black hole via the relations

$$\begin{aligned} M_T &= M + \alpha r_0^{-1-3\omega_q}\left[\frac{r_0}{2}-\frac{(r_0^2+a^2)\arctan(a/r_0)}{a}\right], \\ J_T &= J + \alpha r_0^{-1-3\omega_q}\left[ar_0+\frac{r_0^3}{2a}-\frac{(r_0^2+a^2)\arctan(a/r_0)}{4a^2}\right]. \end{aligned} \tag{3}$$

In the absence of the quintessential matter, $\alpha = 0$, the line element and other quantities reduce to those of a Kerr black hole. To differentiate black holes from naked singularities, in this section we express the black hole parameters and

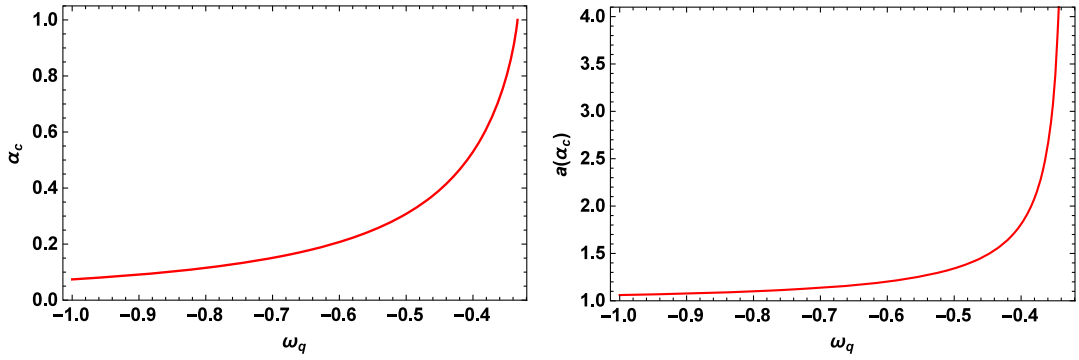

FIG. 1. The figure shows that with increasing ω_q the critical values of the quintessential α_c and spin a_c parameters increase. If $\omega_q \to -1$, we have $\alpha_c \to 2/27$, $a_c(\alpha_c) \to 3/2\sqrt{2}$, and if $\omega_q \to -1/3$, we have $\alpha_c \to 1$ and $a_c(\alpha_c) \to \infty$.

radial distance in units of the gravitational mass, $a/M \to a$, $\alpha M^{-1-3\omega_q} \to \alpha$, $r/M \to r$, and suppose $b = 1\text{–}3\omega_q$. Note that the event horizon must be a null surface. Since an RKBH is a stationary spacetime, the normal to the stationary surface must be proportional to $\partial_\alpha r$ and such a surface is null if $g^{\alpha\beta}(\partial_\alpha r)(\partial_\beta r) = g^{rr} = 0$. Thus, the event horizons are the roots of

$$\Delta = r^2 - 2r + a^2 - \alpha r^b = 0. \tag{4}$$

The locations of the ergospheres are determined by the roots of $r^2 + a^2\cos^2\theta - 2r - \alpha r^b = 0$. The horizons and ergospheres completely depend on the choice of the black hole parameters. For example, if we choose $\omega_q = -2/3$, then Eq. (4) is a cubic equation and has three different real, three identical real, or one real and two complex roots, depending on whether the discriminant $\delta = (36 - 27\alpha a^2)\alpha a^2 - 4a^2 - 32\alpha + 4$ is positive, zero, or negative, respectively. Henceforth, the line element (1) represents a black hole, an extremal black hole, or a naked singularity, respectively.

Generalizing the method used for the case $\omega_q = -2/3$ in Ref. [22], we parametrize the spin parameter as a function of r and α,

$$a^2(\alpha, r) = \alpha r^b - r^2 + 2r. \tag{5}$$

The spin parameter has extrema for $\alpha = \alpha_e$, given by

$$\alpha_e(r) = \frac{2(r-1)}{b r^{b-1}}. \tag{6}$$

The extremum of α_e (denoted by α_c) is located at $r = (b-1)/(b-2)$. So, the critical value of the quintessential parameter (α_c) and the corresponding spin parameter (a_c) are given by

$$\alpha_c = \frac{2(b-2)^{b-2}}{b(b-1)^{b-1}}, \qquad a_c(\alpha_c) = \frac{b-1}{\sqrt{b(b-2)}}. \tag{7}$$

In terms of ω_q, Eq. (7) takes the form

$$\alpha_c = \frac{2(-1-3\omega_q)^{-1-3\omega_q}}{(1-3\omega_q)(-3\omega_q)^{-3\omega_q}}, \qquad a_c(\alpha_c) = \frac{-3\omega_q}{\sqrt{9\omega_q^2 - 1}}. \tag{8}$$

For $\omega_q = -2/3$, we get $\alpha_c = 1/6$ and $a_c(1/6) = 2/\sqrt{3}$ [22]. The expression for the critical value of the quintessential parameter α_c given by Eq. (23) in Ref. [23] is incorrect, because with their expression for $\omega_q = -1/2$ the critical value is $\sqrt{2}/5$ (≈ 0.28284). But, if we choose $\alpha = 0.29 > \sqrt{2}/5$ and $a = 1.2$, the spacetime (1) represents a black hole with three horizons. On the other hand, with our expression (8), for $\omega_q = -1/2$, α_c is equal to $8/15\sqrt{3}$ (≈ 0.30792) and for any value of $\alpha > \alpha_c$ there does not exist a spin parameter a for which Eq. (1) represents a black hole spacetime. Thus, the corrected critical value of the quintessential parameter is given by Eq. (8). The critical values α_c and a_c versus ω_q are shown in Fig. 1, which shows that as ω_q increases, both α_c and a_c increase. Further, when $\omega_q \to -1$, $\alpha_c \to 2/27$, we find $a_c(\alpha_c) \to 3/2\sqrt{2}$, that is, for small ω_q both α_c and a_c are finite. On the other hand, when $\omega_q \to -1/3$, $\alpha_c \to 1$, we have $a_c(\alpha_c) \to \infty$, which means that in the presence of the quintessential field with $\omega_q \approx -1/3$ and $\alpha \approx 1$ a highly spinning black hole is formed.

A. Black holes, extremal black holes, and naked singularities

In this subsection, we will discuss black holes, extremal black holes, and naked singularities, represented by the line element (1). The extrema of Δ can be obtained from the condition

$$\frac{d\Delta}{dr} = 2(r-1) - \alpha(1-3\omega_q)r^{-3\omega_q} = 0. \tag{9}$$

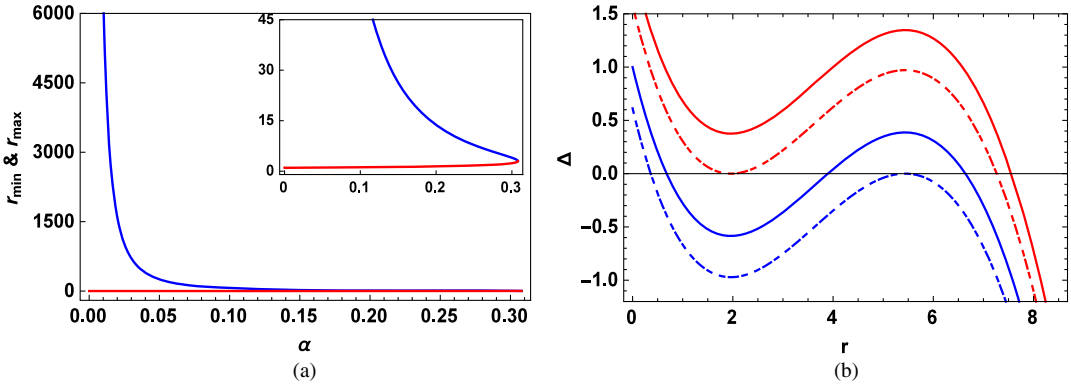

FIG. 2. (a) In this panel we plot $r_{\rm min}$ (red curve) and $r_{\rm max}$ (blue curve) against the parameter α, which shows that $r_{\rm max}$ decreases as α increases, while $r_{\rm min}$ increases as α increases. The inset shows the variation on a smaller scale, from which we can see that $r_{\rm min}$ and $r_{\rm max}$ coincide for $\alpha_c = 8/15\sqrt{3}$. (b) In this panel we plot Δ against r for $\alpha = 0.29$ and different values of a. The blue curve (plotted for $a = 0.9$) shows a black hole with three horizons r_-, r_+, and r_q. The extreme black hole of Type 1 (with $a = 1.258693$), when $r_- = r_+$, is represented by the dashed red curve. The extreme black hole of Type 2 (with $a = 0.782936$), when $r_+ = r_q$, is represented by the dashed blue curve. The red curve represents a naked singularity (with $a = 1.3$) with one horizon r_q only.

For any value of ω_q, Eq. (9) has two real roots denoted by $r_{\rm max}$ and $r_{\rm min}$. Let us denote the corresponding extreme values of the spin parameter a by a_c and $\bar{a}_c$, that is,

$$a_c = \sqrt{\alpha r_{\rm min}^{1-3\omega_q} - r_{\rm min}^2 + 2r_{\rm min}} \quad \text{and}$$
$$\bar{a}_c = \sqrt{\alpha r_{\rm max}^{1-3\omega_q} - r_{\rm max}^2 + 2r_{\rm max}}. \tag{10}$$

Now, we first develop our discussion for values of ω_q for which Eq. (9) can be solved analytically, and then we summarize the results for other values.

1. $\omega_q = -1/2$

For $\omega_q = -1/2$, Eq. (9) becomes

$$\frac{5}{2}\alpha r^{3/2} - 2r + 2 = 0 \tag{11}$$

and can be solve analytically. This equation has two real positive roots for $\alpha \le \alpha_c = 8/15\sqrt{3}$, given by

$$r_{\rm min} = \left(\frac{4}{15\alpha} + \sqrt{3}{\rm Im}(u) - {\rm Re}(u)\right)^2 \quad \text{and}$$
$$r_{\rm max} = \left(\frac{4}{15\alpha} + 2{\rm Re}(u)\right)^2, \tag{12}$$

with

$$u = \frac{1}{15\alpha}\left[2\left(32 - 675\alpha^2 + 15\sqrt{3(675\alpha^2 - 64)}\right)\right]^{1/3}, \tag{13}$$

where ${\rm Re}(u)$ and ${\rm Im}(u)$ represent the real and imaginary parts of u, respectively. These values play an important role in distinguishing black holes from naked singularities. Note that for any value of $\alpha \le \alpha_c = 8/15\sqrt{3}$, there are three real positive roots of Eq. (11), r_-, r_+, and r_q, representing, respectively, the inner, event, and outer horizons of the black hole. These horizons and extrema of Δ given by Eq. (12) satisfy the relation $r_- \le r_{\rm min} \le r_+ \le r_{\rm max} \le r_q$. From Fig. 2(a), one can see that for small α, $r_{\rm max}$ becomes very large and hence we conclude that the quintessential horizon r_q is very large, while as α increases its size decreases. On the other hand, as α increases, $r_{\rm min}$ increases and hence the size of the event horizon increases, although very slowly. Further, if one of the equalities holds—that is, if either $r_{\rm min}$ or $r_{\rm max}$ becomes the horizon of the black hole—Eq. (1) represents an extremal black hole.

The extremal black hole can be one of three types.

Type 1: The first type of extremal black hole exists when $r_{\rm min}$ is the horizon of the black hole, for which $\Delta(r_{\rm min}) = 0$. Here, the inner and event horizons merge into a single horizon, that is, $r_- = r_+$.[1] For this type of black hole the spin parameter satisfies the condition

$$a_c = \sqrt{\alpha r_{\rm min}^{5/2} - r_{\rm min}^2 + 2r_{\rm min}}, \tag{14}$$

where $r_{\rm min}$ is given by Eq. (12). This case is shown by the red dashed curve in Fig. 2(b).

Type 2: The second type of extremal black hole exists when $r_{\rm max}$ is the horizon of the black hole, where $\Delta(r_{\rm max}) = 0$. In this case, the event and outer horizons merge into a single horizon, that is, $r_+ = r_q$. This type of

[1]In Ref. [22] [cf. Eq. (40)], for the case with $\omega_q = -2/3$, it was claimed that the other extremum of Δ ($r_{\rm max}$ in our case) is the outer horizon of the black hole. But this is not true in general and $r_{\rm max} < r_q$ as shown in Fig. 2(b).

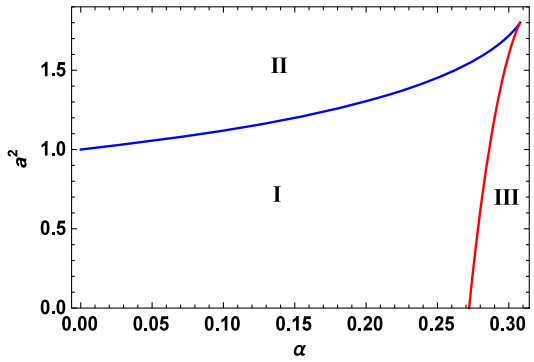

FIG. 3. Region I represents black holes with three horizons. The boundary of Regions I and II represents extremal black holes of Type 1 and the boundary of Regions I and III represents extremal black holes of Type 2. From the figure we can see that $\bar{a}_c$ is defined only for $0.272166 < \alpha < 0.307920$. Thus, Eq. (1) represents extremal black holes of Type 2 only for these values of α. For values of α and a at the point of intersection of these curves, Eq. (1) represents super extremal black holes. For all values of α and a^2 in Regions II and III, Eq. (1) represents naked singularities.

extremal black hole is formed when the rotation parameter satisfies the condition

$$\bar{a}_c = \sqrt{\alpha r_{\rm max}^{5/2} - r_{\rm max}^2 + 2r_{\rm max}}, \tag{15}$$

where $r_{\rm max}$ is given by Eq. (12). This case is shown by the dashed blue curve in Fig. 2(b). In addition, in this case $r_- < r_{\rm min}$. Note that the value of $\bar{a}_c$ is defined only for $0.27216 < \alpha < 0.30792$ (this can be see from the red curve in Fig. 3). So, this type of extremal black hole exists only for these values of α.

Type 3: The third type of extremal black hole exists when all three horizons merge into a single horizon. In this case, we have $r_{\rm min} = r_{\rm max}$, which is possible for

$$\alpha = \alpha_c = \frac{8}{15\sqrt{3}} \quad \text{and} \quad a_c = \bar{a}_c = \frac{3}{\sqrt{5}}. \tag{16}$$

This type of black hole is known as a super-extremal black hole.

Finally, we conclude that for any value of $\alpha < \alpha_c$ and the corresponding spin parameter $a < a_c$, Eq. (1) can represent a black hole with three different horizons. For any given value of α with $\alpha < \alpha_c$, the line element (1) represents an extremal black hole of Type 1 or Type 2, depending on whether the spin parameter $a = a_c(\alpha)$ or $a = \bar{a}_c(\alpha)$. For $\alpha = \alpha_c$ and $a = a_c(\alpha_c)$, the spacetimes of Eq. (1) represent super-extremal black holes. For any other possibilities, the spacetimes represent naked singularities. In Fig. 3, we plot $a = a_c$ (blue curve) and $a = \bar{a}_c$ (red curve) in the (α, a^2) plane, which divide the whole plane into three different regions. In Region I, Eq. (1) represents a black hole, whereas in Regions II and III it represents a naked singularity. For all points on the boundary of Regions I and II, Eq. (1) represents an extremal black hole of Type 1, and on the boundary of Regions II and III, Eq. (1) represents an extremal black hole of Type 2.

2. When $\omega_q = -4/9$

Again, for $\omega_q = -4/9$, Eq. (9) can be solved analytically. In this case $\alpha_c \approx 0.404975$ and for all $\alpha \le \alpha_c$ Eq. (9) has two real positive roots,

$$r_{\rm min} = \left(\frac{3}{14\alpha} + \frac{v}{2} - \frac{1}{2}\sqrt{\frac{27}{49\alpha^2} - v^2 + \frac{54}{343\alpha^3 v}}\right)^3,$$
$$r_{\rm max} = \left(\frac{3}{14\alpha} + \frac{v}{2} + \frac{1}{2}\sqrt{\frac{27}{49\alpha^2} - v^2 + \frac{54}{343\alpha^3 v}}\right)^3, \tag{17}$$

with

$$v = \sqrt{\frac{9}{49\alpha^2} + \frac{2^{2/3}(27 + \sqrt{729 - 10976\alpha^3})^{1/3}}{7\alpha} + \frac{2^{7/3}}{(27 + \sqrt{729 - 10976\alpha^3})^{1/3}}}. \tag{18}$$

We then obtain the extreme values of the spin parameter corresponding to these two solutions,

$$a_c = \sqrt{\alpha r_{\rm min}^{7/3} - r_{\rm min}^2 + 2r_{\rm min}} \quad \text{and}$$
$$\bar{a}_c = \sqrt{\alpha r_{\rm max}^{7/3} - r_{\rm max}^2 + 2r_{\rm max}}, \tag{19}$$

where $r_{\rm min}$ and $r_{\rm max}$ are given by Eq. (17). From Fig. 4(a), we can see that as α increases, $r_{\rm min}$ increases and $r_{\rm max}$ decreases. Thus, due to the relation $r_- \le r_{\rm min} \le r_+ \le r_{\rm max} \le r_q$, in this case we can also conclude that as α increases, the size of the event horizon increases, while that of the outer horizon decreases. For $\alpha < \alpha_c$ and $a < a_c$, Eq. (1) represents a black hole with three horizons [as shown by the blue curve in Fig. 4(b)]. For $\alpha < \alpha_c$, and $a = a_c$ or $a = \bar{a}_c$, Eq. (1) represents an extremal black hole of Type 1 or Type 2 [as shown by the dashed red and the dashed blue curve in Fig. 4(b)]. Further, Fig. 5 shows that extremal black holes of Type 2 exist only for $0.375 < \alpha < 0.404975$. For any other possibilities [that is, for any (α, a^2) in Regions II or III

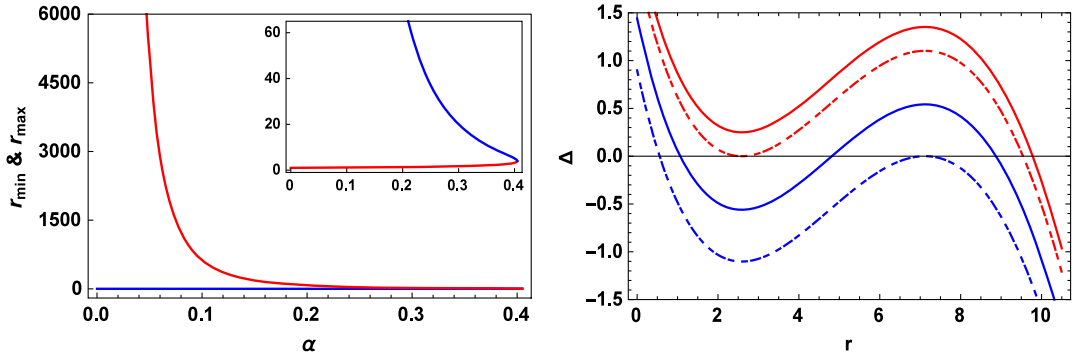

FIG. 4. (a) In this panel we plot $r_{\min}$ (red curve) and $r_{\max}$ (blue curve) against the parameter α which shows that $r_{\max}$ decreases as α increases, while $r_{\min}$ increases as α increases. The inset shows the variation on a smaller scale, from which we can see that $r_{\min}$ and $r_{\max}$ coincide for $\alpha_c = 0.404975$. (b) In this panel we plot Δ against r for $\alpha = 0.383$ and different values of a. The blue curve (plotted for $\alpha = 1.2$) shows a black hole with three horizons r_-, r_+, and r_q. The dashed red curve (plotted for $a = 1.41428$) represents an extremal black hole of Type 1 when $r_- = r_+$. The dashed blue curve (plotted for $a = 0.947639$) represents an extremal black hole of Type 2 when $r_+ = r_q$. The red curve (plotted for $a = 1.5$) represent a naked singularity with one horizon r_q only.

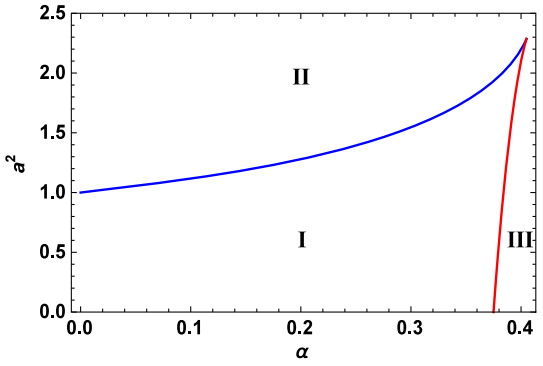

FIG. 5. Region I represents a black hole with three horizons. The boundary of region I and II represents an extremal black hole of Type 1 and the boundary of region I and II represents an extremal black hole of Type 2. The figure shows that an extremal black hole of Type 2 exists only for $0.375 < \alpha < 0.404975$. For the values in regions II and III, the spacetime (1) represents a naked singularity.

of Fig. 5], the line element (1) represents a naked singularity.

By numerical analysis we see that the behavior is the same for all values of $-1 < \omega_q < -1/3$, that is, Eq. (1) represents a black hole, provided that $\alpha \le \alpha_c$ and $a \le a_c$. By increasing α, the size of the quintessential horizon decreases, while that of event horizon increases. Further, the types of extremal black holes and the conditions for some values of ω_q are summarized in Tables I and II.[2]

[2]The values $\bar{\alpha}_c$ in Table I also play an important role in a Kiselev black hole. For any chosen ω_q, $\alpha = \bar{\alpha}_c$ is the critical value for a Kiselev black hole. The line element only represents a Kiselev black hole for $\alpha \le \bar{\alpha}_c$.

III. SPIN PRECESSION OF A TEST GYROSCOPE IN AN RKBH

In this section, we will discuss the spin precession frequency of a test gyroscope attached to a stationary observer in an RKBH. A stationary observer is an observer who remains at fixed r and θ coordinates by rotating around the black hole (with respect to observers at infinity) in the same sense as the black hole's rotation. The 4-velocity of such an observer is $[u^\mu] = u^t(1,0,0,\Omega)$, where $\Omega = d\phi/dt$. Consider a test gyroscope attached to a stationary observer moving along a Killing trajectory in an RKBH (stationary spacetime). The RKBH spacetime admits two Killing vectors: the time translation Killing vector ∂_t and the azimuthal Killing vector ∂_ϕ. The vector $K = \partial_t + \Omega\partial_\phi$ is also a Killing vector. The 1-form of the general spin precession frequency can be expressed as [36]

$$\tilde{\Omega}_p = \frac{1}{2K^2} * (\tilde{K} \wedge d\tilde{K}), \tag{20}$$

where $\tilde{K}$ is the corresponding covector of K, $*$ represents the Hodge dual, and $\wedge$ is the wedge product. Thus, the spin precession frequency of a timelike stationary observer with an angular velocity Ω with respect to a fixed star in a stationary axisymmetric spacetime is given by [34]

$$\begin{aligned}\vec{\Omega}_p = {} & \frac{\varepsilon_{ckl}}{2\sqrt{-g}(1 + 2\Omega\frac{g_{0c}}{g_{00}} + \Omega^2\frac{g_{cc}}{g_{00}})} \\ & \times \left[\left(g_{0c,k} - \frac{g_{0c}}{g_{00}}g_{00,k}\right) + \Omega\left(g_{cc,k} - \frac{g_{cc}}{g_{00}}g_{00,k}\right)\right. \\ & \left. + \Omega^2\left(\frac{g_{0c}}{g_{00}}g_{cc,k} - \frac{g_{cc}}{g_{00}}g_{0c,k}\right)\right]\partial_l,\end{aligned} \tag{21}$$

TABLE I. Critical values of the quintessential parameter α and spin parameter a for different ω_q.

ω_q	$-4/9$	$-1/2$	$-5/9$	$-2/3$	$-7/9$	$-8/9$
α_c	0.404975	0.30792	0.244298	0.166667	0.121934	0.0934523
$\bar{\alpha}_c$	0.375	0.2721655269759	0.2051971136011	0.125	0.0806490313479	0.053963051556
$a(\alpha_c)$	1.51186	1.34164	1.25	1.1547	1.1068	1.07872

where g is the determinant of the metric $g_{\mu\nu}$ and ε_{ckl} is the Levi-Civita symbol. This expression is valid for observers both inside and outside of the ergosphere for a restricted range of Ω, such that its velocity $u^\nu = u^t(1,0,0,\Omega)$ remains timelike. Substituting the metric coefficients from Eq. (1) into Eq. (21), we get

$$\vec{\Omega}_p = \frac{(F\sqrt{\Delta}\cos\theta)\hat{r} + (H\sin\theta)\hat{\theta}}{\Sigma^{3/2}[\Sigma - (2Mr+\alpha r^b) + 2\Omega a\sin^2\theta(2Mr+\alpha r^b) - \Omega^2\sin^2\theta\{(r^2+a^2)\Sigma + a^2\sin^2\theta(2Mr+\alpha r^b)\}]}, \tag{22}$$

with

$$\begin{aligned}
F &= a(2Mr+\alpha r^b) - \frac{\Omega}{8}[8r^4 + 3a^4 + 8a^2r^2 + 16a^2Mr + 4a^2(2\Delta - a^2)\cos 2\theta + a^4\cos 4\theta] \\
&\quad + \Omega^2 a^3\sin^4\theta(2Mr+\alpha r^b), \\
H &= a\left[M(r^2 - a^2\cos^2\theta) + \frac{\alpha}{2}r^{b-1}\{(2-b)r^2 - ba^2\cos^2\theta\}\right] \\
&\quad + \Omega[r(r^4 + a^4\cos^4\theta + 2r^2a^2\cos^2\theta) - r(r^2 + a^2\cos^2\theta)(2Mr+\alpha r^b) + (r^2 + a^2 + a^2\sin^2\theta) \\
&\quad \times\left\{-Mr^2 + \left(M + \frac{\alpha}{2}br^{b-1}\right)a^2\cos^2\theta + \frac{\alpha}{2}(b-2)r^{b+1}\right\}\Big] + a\Omega^2\sin^2\theta[r^3(2Mr+\alpha r^b) + ra^2\cos^2\theta(2Mr+\alpha r^b) \\
&\quad + Mr^4 + Mr^2a^2 - (r^2+a^2)\left(M + \frac{\alpha}{2}br^{b-1}\right)a^2\cos^2\theta - \frac{\alpha}{2}(r^2+a^2)(b-2)r^{b+1}\Big],
\end{aligned} \tag{23}$$

where $b = 1$–$3\omega_q$ and $\hat{r}$, $\hat{\theta}$ are the basis vectors in the r and θ directions, respectively. Setting $\alpha = 0$ gives the spin precession for a Kerr black hole [34]. In the above expression for timelike observers, Ω has the restriction

$$\Omega_-(r,\theta) < \Omega(r,\theta) < \Omega_+(r,\theta), \tag{24}$$

where

TABLE II. The conditions for different types of extremal black holes.

Type	Horizons	Condition	Range of α	Condition of a
1	$r_- = r_+$	$\Delta(r_{\min}) = 0$	$\alpha < \alpha_c$	$a = a_c$
2	$r_+ = r_q$	$\Delta(r_{\max}) = 0$	$\bar{\alpha}_c < \alpha < \alpha_c$	$a = \bar{a}_c$
3	$r_- = r_+ = r_q$	$r_{\min} = r_{\max}$	$\alpha = \alpha_c$	$a = a(\alpha_c)$

$$\Omega_\pm = \frac{a\sin\theta(2M\alpha + \alpha r^b) \pm \Sigma\sqrt{\Delta}}{\sin\theta[(r^2+a^2)\Sigma + a^2\sin^2\theta(2Mr+\alpha r^b)]}. \tag{25}$$

This expression shows that for an observer close to the horizon as well as to the ring singularity $(r = 0, \theta = \pi/2)$, Ω_+ and Ω_- coincide. Thus, no timelike observer can exist at these points and the expression for $\vec{\Omega}_p$ is not a valid expression at these points, but it is still useful when discussing precession in the limit of these points.

A. LT precession frequency

The precession frequency $(\vec{\Omega}_p)$ given by Eq. (22) is the general precession frequency of a gyroscope with angular velocity Ω. The precession frequency includes effects due to both spacetime rotation (LT precession) and curvature (geodetic precession). If we set $\Omega = 0$, then $\vec{\Omega}_p$ reduces to the LT precession $(\Omega_{\rm LT})$ frequency of the gyroscope attached to a static observer, who can exist only outside the ergosphere. The expression for the LT precession frequency is

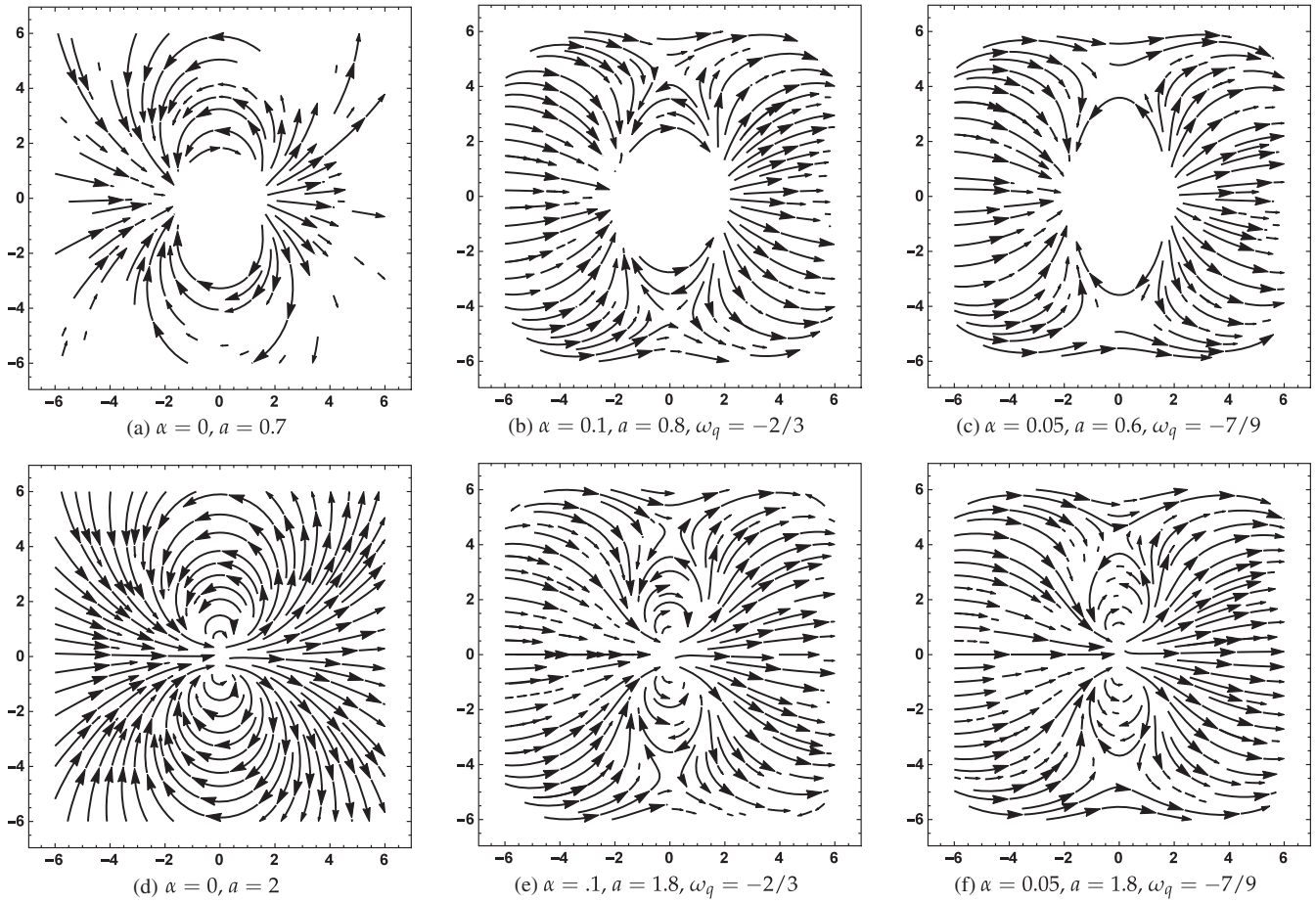

FIG. 6. The vector field of the LT precession frequency [24] for black holes (a)–(c) and naked singularities (d)–(f) for different values of α [in the Cartesian plane corresponding to (r, θ)]. The field lines show that for a black hole the vector field is only defined outside the ergosphere, while for a naked singularity it is finite up to the ring singularity.

$$\vec{\Omega}_{\rm LT} = a\frac{[(2Mr+\alpha r^b)\sqrt{\Delta}\cos\theta]\hat{r} + [\{M(r^2 - a^2\cos^2\theta) + \frac{a}{2}r^{b-1}((2-b)r^2 - ba^2\cos^2\theta)\}\sin\theta]\hat{\theta}}{(r^2 + a^2\cos^2\theta)^{3/2}(r^2 - 2Mr + a^2\cos^2\theta - \alpha r^b)}. \tag{26}$$

We plot the vector field of the LT precession frequency (26) for black holes and naked singularities for different values of α [in the Cartesian plane corresponding to (r, θ)] in the first and second rows of Fig. 6, respectively. It can be seen that for black holes the LT precession frequency diverges if the observer approaches the ergosphere along any direction. However, outside the ergosphere the frequency is finite everywhere. For naked singularities it is regular throughout the whole region except at the ring singularity ($r = 0, \theta = \pi/2$). This is because the denominator of Eq. (26) goes to zero at the ergospheres and ring singularity. Further, for black holes the field lines at the pole precess in the same direction as the black hole rotation, while those on the equatorial plane precess in the opposite sense as in the case of a linearized gravitation field [28]. The magnitude of the LT precession frequency is

$$\Omega_{\rm LT} = \frac{a\sqrt{(2Mr+\alpha r^b)^2|\Delta|\cos^2\theta + (M(r^2 - a^2\cos^2\theta) + \frac{a}{2}r^{b-1}\{(2-b)r^2 - ba^2\cos^2\theta\})^2\sin^2\theta}}{(r^2 + a^2\cos^2\theta)^{3/2}|r^2 + a^2\cos^2\theta - 2Mr - \alpha r^b|}. \tag{27}$$

The LT precession frequency for a Kerr black hole has already been obtained for $\alpha = 0$ [35]. The magnitude of the LT precession frequency for different values of ω_q is plotted in Fig. 7(a). The LT precession frequency for black holes ($\omega_q = -4/9$) diverges at the ergosphere, and for naked singularities ($\omega_q = -2/3, \omega_q = -5/9, \omega_q = -1/2$) it remains finite. Further, from Fig. 7(b) we can see that for fixed α, ω_q, and a, for naked singularities $\Omega_{\rm LT}$ increases with increasing angle and has a peak. The peak increases with increasing angle, and due to the ergosphere in the naked singularity case it blows up, as in the case of a Kerr black hole [35].

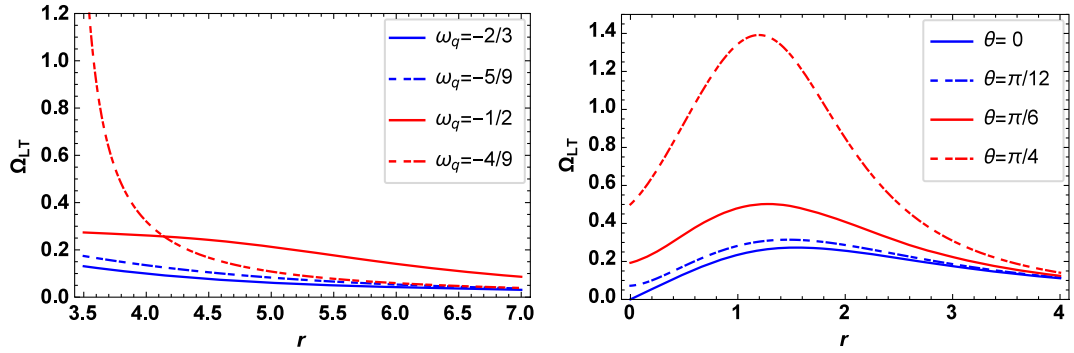

(a) $\alpha = 0.3, a = 0.1, \theta = \pi/3$ (b) $\alpha = 0.2, a = 2, \omega_q = -4/9$

FIG. 7. (a) The magnitude of the LT precession frequency Ω_{LT} (in M^{-1}) versus r (in M). The figure shows that for fixed θ, α, and a, the LT precession frequency remains finite for naked singularities with $\omega_q = -2/3, -5/9, -1/2$, while it blows up for black holes with $\omega_q = -4/9$ as the observer reaches the ergosphere. Further, for a naked singularity, as ω_q increases the magnitude of Ω_{LT} increases. (b) In this panel we plot the magnitude of Ω_{LT} for a naked singularity, which shows that it is regular throughout the region.

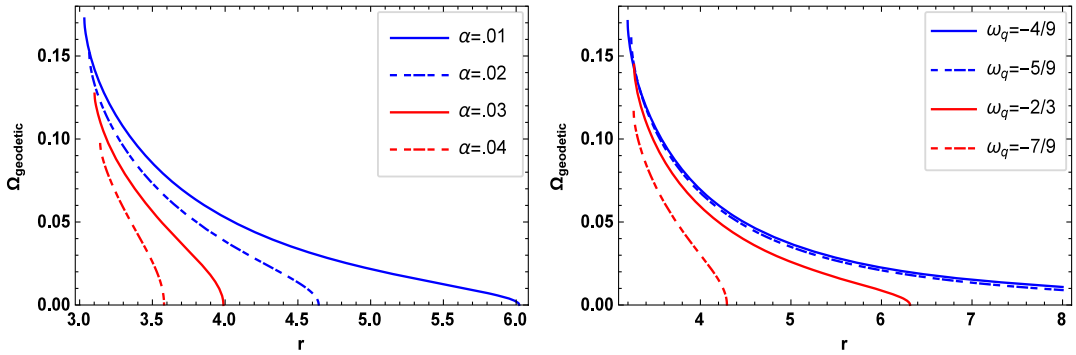

FIG. 8. (a) In this panel we plot the geodetic precession $\Omega_{geodetic}$ versus r for $M = 1$ and $\omega_q = -8/9$. The figure shows that as α increases, the magnitude of $\Omega_{geodetic}$ in a circular orbit decreases. (b) In this panel we plot the geodetic precession against r for $\alpha = 0.05$ and different values of ω_q, which shows that as ω_q increases, $\Omega_{geodetic}$ in a fixed orbit increases. Further, for fixed ω_q and α, the geodetic precession decreases as the radius of the circular orbit increases.

B. Geodetic precession

If we set the spin parameter $a = 0$ in the line element (1), it reduces to a KBH [5], in which the LT precession frequency vanishes. However, for $a = 0$ the precession frequency (22) is nonzero. This precession is due to the curvature of the spacetime and is known as geodetic precession. It is given by

$$\vec{\Omega}_p|_{a=0} = \Omega \frac{[-(r^2 - 2Mr - \alpha r^b)\cos\theta]\hat{r} + [(r - 3M + \frac{\alpha}{2}(b-4)r^{b-1})\sin\theta]\hat{\theta}}{r - (2M + \alpha r^{b-1}) - r^3\Omega^2\sin^2\theta}. \tag{28}$$

As the KBH spacetime is spherically symmetric, the geodetic frequency is the same over the spherical surface around the black hole, so without loss of generality we can set $\theta = \pi/2$. In the equatorial plane for any circular orbit of radius r the angular frequency Ω of an observer is equal to its Kepler frequency Ω_{Kep}, that is, $\Omega = \Omega_{Kep} = \sqrt{\frac{M}{r^3} + \frac{\alpha}{2}(2-b)r^{b-4}}$, and the magnitude of Eq. (28) is given by

$$\Omega_p|_{a=0,\Omega=\Omega_{Kep}} = \Omega = \sqrt{\frac{M}{r^3} + \frac{\alpha}{2}(2-b)r^{b-4}}. \tag{29}$$

The above expression is the precession frequency in the Copernican frame, computed with respect to the proper time τ. The proper time τ, measured in the Copernican frame, is related to the coordinate time t via

$$d\tau = \sqrt{1 - \frac{3M}{r} + \frac{\alpha}{2}(b-4)r^{b-2}}dt,$$

and we can obtain the geodetic precession frequency in the coordinate basis as

$$\Omega' = \sqrt{\left(\frac{M}{r^3} + \frac{\alpha}{2}(2-b)r^{b-4}\right)\left(1 - \frac{3M}{r} + \frac{\alpha}{2}(b-4)r^{b-2}\right)}.$$

In terms of ω_q, the geodetic precession frequency[3] is [32]

$$\Omega' = \sqrt{\left(\frac{M}{r^3} + \frac{\alpha}{2}(1+3\omega_q)r^{-3(1+\omega_q)}\right)\left(1 - \frac{3M}{r} - \frac{3\alpha}{2}(1+\omega_q)r^{-(1+3\omega_q)}\right)}. \tag{30}$$

Now, after a complete revolution of the observer around the black hole, the frequency associated with the change in the angle of the spin vector is given by

$$\Omega_{\text{geodetic}} = \sqrt{\frac{M}{r^3} + \frac{\alpha}{2}(1+3\omega_q)r^{-3(1+\omega_q)}}\left(1 - \sqrt{1 - \frac{3M}{r} - \frac{3\alpha}{2}(1+\omega_q)r^{-(1+3\omega_q)}}\right). \tag{31}$$

For $\alpha = 0$, we obtain the geodetic precession of a Schwarzschild black hole [30,31]. The geodetic precession frequency is plotted in Fig. 8, which shows that for fixed ω_q, as α increases the magnitude of the geodetic precession in a circular orbit decreases [see Fig. 8(a)], whereas for fixed α, as ω_q increases the magnitude increases. In addition, for fixed ω_q and α, the geodetic precession decreases as the radius of the circular orbit increases [see Fig. 8(b)].

IV. DISTINGUISHING RKBHs FROM NAKED SINGULARITIES USING THE PRECESSION OF A TEST GYROSCOPE

In this section, using the precession frequency of a test gyroscope attached to a stationary observer, we will differentiate RKBHs from naked singularities. The expression for the precession frequency is given in Eq. (22). For timelike stationary observers the angular velocity has the restricted range (24). The angular velocity Ω in terms of $\Omega_\pm$ can be written as

$$\Omega = k\Omega_+ + (1-k)\Omega_-, \tag{32}$$

where $0 < k < 1$ and $\Omega_\pm$ is defined by Eq. (25). Using Eq. (24) in Eq. (32) yields

$$\Omega = \frac{a\sin\theta(2Mr + \alpha r^b) - (1-2k)\Sigma\sqrt{\Delta}}{\sin\theta[(r^2+a^2)\Sigma + a^2\sin^2\theta(2Mr+\alpha r^b)]}. \tag{33}$$

[3]It should be noted that the geodetic precession frequency obtained in Ref. [32] has a factor of 2 error.

For $k = 1/2$, the angular velocity becomes

$$\Omega = \frac{a\sin\theta(2Mr + \alpha r^b)}{\sin\theta[(r^2+a^2)\Sigma + a^2\sin^2\theta(2Mr+\alpha r^b)]} = -\frac{g_{t\phi}}{g_{\phi\phi}}. \tag{34}$$

An observer with this angular velocity is called a zero-angular-momentum observer (ZAMO). The precession frequency of a gyroscope attached to a ZAMO in the Kerr black hole spacetime behaves differently than that of gyroscopes attached to other observers with angular velocities different than that of a ZAMO [34]. These gyros are nonrotating with respect to the local geometry and stationary observers regard both $+\phi$ and $-\phi$ [37,38]. Thus, it is interesting to study how the precession frequency of a gyroscope attached to a ZAMO behaves in a Kerr black hole surrounded by a quintessential matter field. Using Eq. (33) in Eq. (22), we obtain the precession frequency in terms of the parameter k as

$$\vec{\Omega}_p = \frac{(r^2+a^2)\Sigma + a^2\sin^2\theta(2Mr+\alpha r^b)}{4k(1-k)\rho^7\Delta} \times [(F\sqrt{\Delta}\cos\theta)\hat{r} + (H\sin\theta)\hat{\theta}], \tag{35}$$

where F and H are defined by Eq. (23). Finally, the magnitude of precession frequency is given as

$$\Omega_p = \frac{(r^2+a^2)\Sigma + a^2\sin^2\theta(2Mr+\alpha r^b)}{4k(1-k)\rho^7|\Delta|} \times [F^2|\Delta|\cos^2\theta + H^2\sin^2\theta]^{1/2}. \tag{36}$$

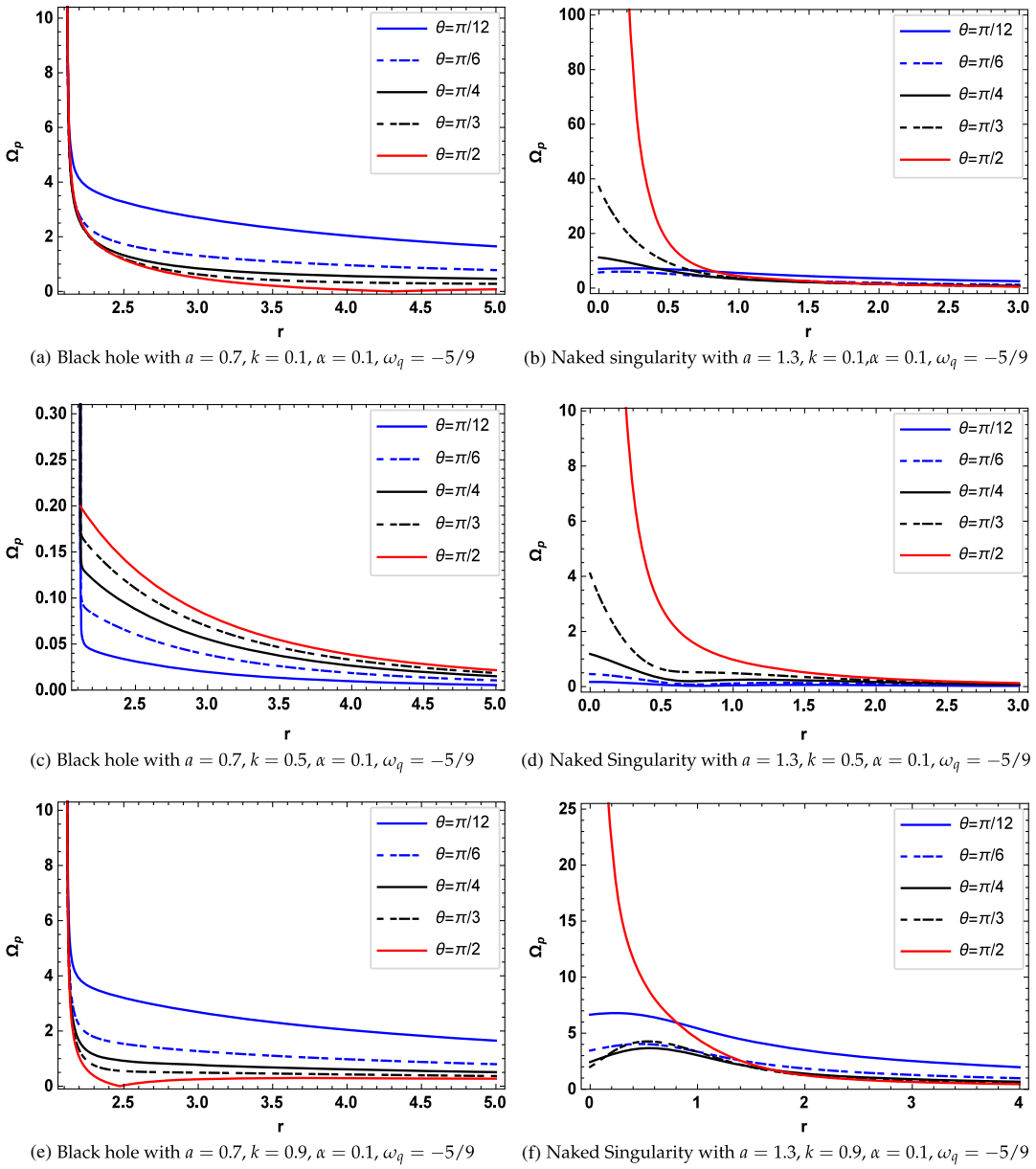

(a) Black hole with $a = 0.7$, $k = 0.1$, $\alpha = 0.1$, $\omega_q = -5/9$

(b) Naked singularity with $a = 1.3$, $k = 0.1$,$\alpha = 0.1$, $\omega_q = -5/9$

(c) Black hole with $a = 0.7$, $k = 0.5$, $\alpha = 0.1$, $\omega_q = -5/9$

(d) Naked Singularity with $a = 1.3$, $k = 0.5$, $\alpha = 0.1$, $\omega_q = -5/9$

(e) Black hole with $a = 0.7$, $k = 0.9$, $\alpha = 0.1$, $\omega_q = -5/9$

(f) Naked Singularity with $a = 1.3$, $k = 0.9$, $\alpha = 0.1$, $\omega_q = -5/9$

FIG. 9. In this figure we plot the magnitude of the spin precession frequency Ω_p (in M^{-1}) versus r (in M) for black holes in the left column and for naked singularities in the right column. For black holes we take $a = 0.7$, $\alpha = 0.1$, $\omega_q = -5/9$ and for naked singularities we take $a = 1.3$, $\alpha = 0.1$, $\omega_q = -5/9$ and $k = 0.1$, 0.5, 0.9 in the first, second, and third rows, respectively. For black holes the precession frequency Ω_p diverges for all $k = 0.1$, 0.5, 0.9 as the observer approaches the event horizon along any direction (except $\theta = \pi/2$ for $k = 0.5$), whereas for naked singularities it remains finite along all directions except at the ring singularity ($r = 0$, $\theta = \pi/2$).

The denominator of the above equation vanishes at the ring singularity and horizons of the black hole. Also from Eq. (35), we can see that the numerator of the radial part of $\vec{\Omega}_p$ goes to zero as the observer approaches the horizons. So, we will study spin precessions when the observer reaches the horizon along different directions with different k, a, ω_q, and α in detail. The magnitude of the precession frequency (36) versus r is plotted for black holes in the left column and for naked singularities in the right column of Fig. 9, for $k = 0.1$, 0.5, 0.9 in the first, second, and third rows, respectively.

For black holes with $a = 0.7$, $\alpha = 0.1$, $\omega_q = -5/9$, the precession frequency for $k = 0.1$ and $k = 0.9$ blows up when the observer approaches the horizon along any given direction [see Figs. 9(a) and 9(e)]. On the other hand, in the case of naked singularities with $a = 1.3$, $\omega_q = -5/9$, $\alpha = 0.1$, it can be seen from the right column of Fig. 9 that the precession frequency for all $k = 0.1$, 0.5, 0.9

remains finite up to $r = 0$ along all directions except $\theta = \pi/2$. Near $r = 0$, $\theta = \pi/2$, the frequency diverges because of the ring singularity, as in the case of a Kerr black hole [34]. However, for a ZAMO ($k = 0.5$) the precession frequency in an RKBH behaves differently than that in a Kerr black hole. For a ZAMO, the precession frequency in a Kerr black hole remains finite as the observer approaches the horizon [34], but for an RKBH it diverges along all directions except $\theta = \pi/2$ [see Fig. 9(c)].

For $k = 0.5$, by inserting Eq. (34) into Eq. (23) we get

$$F|_{k=0.5} = \frac{a^3(2Mr + \alpha r^b)}{8A^2}[8a(2Mr + \alpha r^b)^2 \sin^4\theta + A\{a^2 - 8Mr + 4r^2 + 4\alpha r^b - a^2\cos 4\theta + 4(2Mr - r^2 + \alpha r^b)\cos 2\theta\}], \quad (37)$$

$$H|_{k=0.5} = \frac{-a\Delta\Sigma^2}{4rA^2}[2Mr\{a^4 - 3a^2r^2 - 6r^4 + a^2(a^2 - r^2)\cos 2\theta\} + \alpha r^b\{ba^4 + 3(b-2)a^2r^2 + 2(b-4)r^4 + a^2\{a^2b + r^2(b-2)\}\cos 2\theta\}], \quad (38)$$

where

$$A = (r^2 + a^2)\Sigma + a^2\sin^2\theta(2Mr + \alpha r^b).$$

It is clear from Eqs. (37) and (38) that, as for all other values of k, for $k = 0.5$ near the horizon the angular component of the precession frequency (35) remains finite but its radial component blows up. However, along $\theta = \pi/2$, the radial component is zero and thus along this direction near the

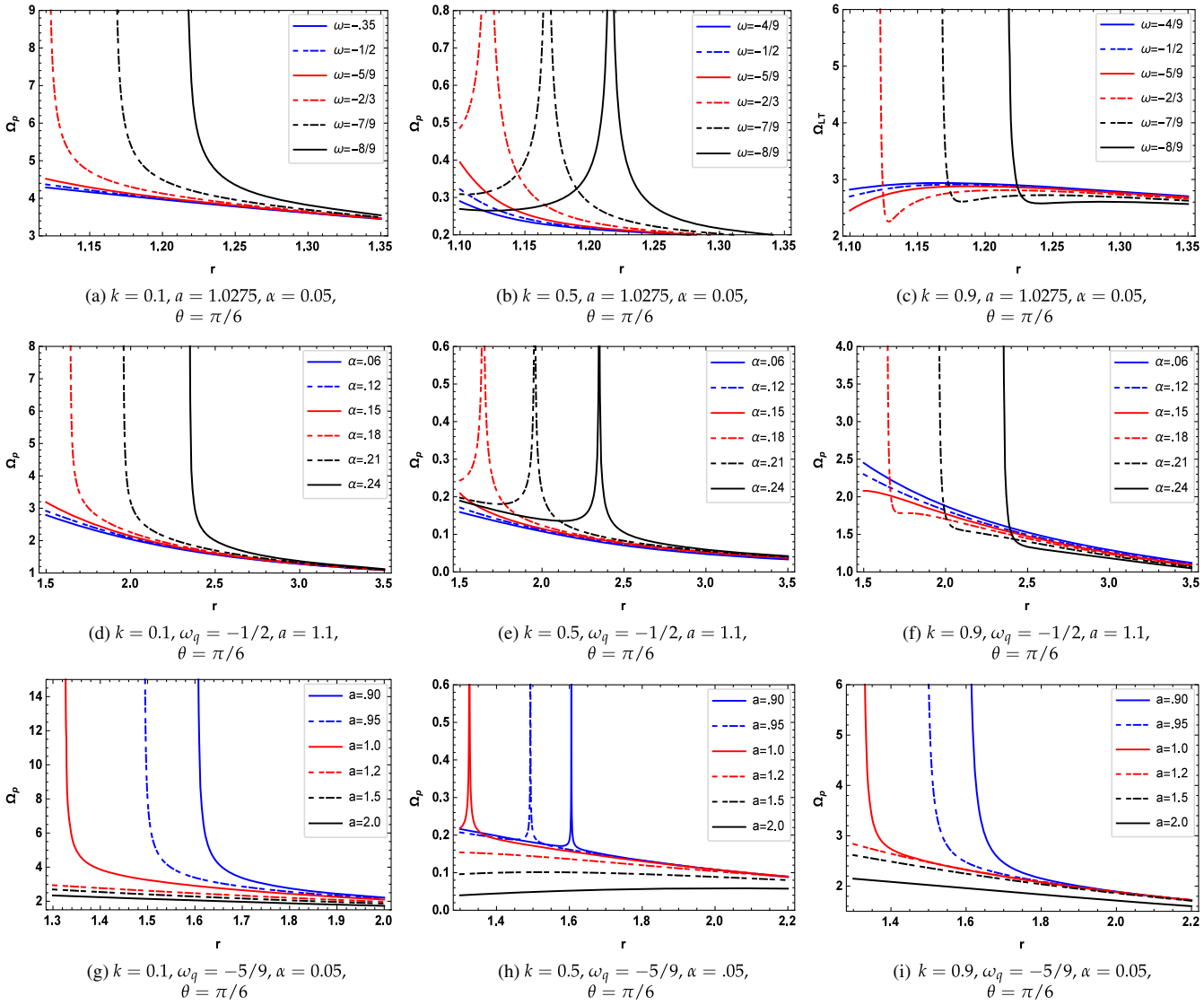

(a) $k = 0.1$, $a = 1.0275$, $\alpha = 0.05$, $\theta = \pi/6$ (b) $k = 0.5$, $a = 1.0275$, $\alpha = 0.05$, $\theta = \pi/6$ (c) $k = 0.9$, $a = 1.0275$, $\alpha = 0.05$, $\theta = \pi/6$

(d) $k = 0.1$, $\omega_q = -1/2$, $a = 1.1$, $\theta = \pi/6$ (e) $k = 0.5$, $\omega_q = -1/2$, $a = 1.1$, $\theta = \pi/6$ (f) $k = 0.9$, $\omega_q = -1/2$, $a = 1.1$, $\theta = \pi/6$

(g) $k = 0.1$, $\omega_q = -5/9$, $\alpha = 0.05$, $\theta = \pi/6$ (h) $k = 0.5$, $\omega_q = -5/9$, $\alpha = .05$, $\theta = \pi/6$ (i) $k = 0.9$, $\omega_q = -5/9$, $\alpha = 0.05$, $\theta = \pi/6$

FIG. 10. The magnitude of the precession frequency Ω_p (in M^{-1}) versus r (in M) for different parameters. The figure shows that for black holes Ω_p diverges near the black hole horizon, while for naked singularities it remains finite.

horizon the precession frequency is finite. On the other hand, for a Kerr black hole, we have

$$F|_{k=0.5,\alpha=0} = \frac{2Mra^3\Delta\Sigma^2\sin^2\theta}{(r^2+a^2)\Sigma + 2Mra^2\sin^2\theta)^2}, \quad (39)$$

$$H|_{k=0.5,\alpha=0} = -\frac{aM\Delta\Sigma^2[a^4 - 3a^2r^2 - 6r^4 + a^2(a^2-r^2)\cos 2\theta]}{2(r^2+a^2)\Sigma + 2Mra^2\sin^2\theta)^2}. \quad (40)$$

From Eq. (36), we can see that in this case the precession frequency remains finite when the observer approaches the black hole along any given direction [34]. The gyroscopes attached to all of the stationary observers (including the ZAMO) in the RKBH behave in the same manner, and the peculiar behavior of the ZAMOs in the Kerr spacetime is avoided.

In Fig. 10, we further illustrate the behavior of the precession frequency for other values of the parameters a, ω_q, and α. In the first, second, and third rows of the figure, Ω_p versus r is plotted for different values of ω_q, α, and a. It can be seen from the first row that for black holes ($\omega_q = -8/9, -7/9, -2/3$) and for all observers ($k = 0.1$, 0.5, 0.9) Ω_p diverges near the horizon. On the other hand, for naked singularities ($\omega_q = -7/20, -1/2, -5/9$) and for all observers ($k = 0.1$, 0.5, 0.9) Ω_p remains finite. In the second row, the behavior of Ω_p for different values of α shows that for all stationary observers ($k = 0.1$, 0.5, 0.9) in the black hole spacetimes ($\alpha = 0.18$, 0.21, 0.24) Ω_p diverges near the horizon, but in the naked singularity spacetimes ($\alpha = 0.06$, 0.12, 0.15) it remains finite in the whole region. In can also be seen that the same behavior is also present for different values of a. That is, for all observers ($k = 0.1$, 0.5, 0.9), the frequency diverges for black holes ($a = 0.90$, 0.95, 1.0), whereas it remains finite for naked singularities.

Finally, using the spin precession, we can differentiate RKBHs from naked singularities. Consider gyroscopes attached to stationary observers with nonzero azimuthal components (Ω) of their four-velocities. These observers move along circles at constant r and θ, with a constant angular velocity Ω. We can find the range of Ω such that their velocities are timelike. In this restricted range, we can define Ω in terms of the parameter k. Consider observers moving along two different directions θ_1 and θ_2. From the precession frequency Ω_p of the stationary observers moving in circular orbits, we conclude that (i) if Ω_p becomes arbitrarily large as an observer approaches the central object in the quintessential field along both θ_1 and θ_2, then the spacetime is a black hole, and (ii) if Ω_p becomes arbitrarily large as an observer approaches the central object for at most one of the two directions, the spacetime will be a naked singularity. For black holes, Ω_p becomes arbitrarily large when an observer approaches the event horizon, which covers the black hole singularity in all directions; therefore, observers approaching the black hole from all directions will see a divergence. However, for naked singularities, this divergence appears only along the ring singularity ($r = 0, \theta = \pi/2$); therefore, only observers along this direction will see the divergence.

V. CONCLUSIONS

In this paper, we presented critical values of the quintessential and spin parameters (α_c and a_c) to distinguish RKBHs from naked singularities. These values are directly proportional to the dimensionless parameter ω_q, which has the range $-1 < \omega_q < -1/3$. We have shown that, if $\omega_q \to -1$, $\alpha_c \to 2/27$, then black holes can form for very small α, and if $\omega_q \to -1/3$, $\alpha_c \to 1$ with $a_c \to \infty$, a highly spinning black hole can form. Further, for all $-1 < \omega_q < -1/3$, the black holes have three, inner, event and outer horizons. We also studied extremal black holes and found the bounds of the horizons. For all ω_q, as α increases the size of the event horizon increases, while the size of the outer horizon decreases. We then studied the critical value of the quintessential parameter $\bar{a}_c$ for a KBH and found the radius of the extremal black holes. Similar to an RKBH, in the case of a KBH, as α increases the size of the event horizon increases, whereas the size of the outer horizon decreases.

We also studied the spin precession frequency of a test gyroscope attached to a timelike stationary observer in the RKBH spacetime. For timelike stationary observers with angular velocity Ω with respect to a fixed star, we found the restricted ranges of Ω. From the precession frequency for static observers ($\Omega = 0$), we obtained the LT precession frequency. For an RKBH, the LT precession frequency diverges as the observer approaches the ergosphere along any direction. On the other hand, for naked singularities it remains finite throughout the whole region except at the ring singularity. From the general precession frequency we then obtained the geodetic precession for observers in a KBH. The magnitude of the geodetic precession frequency in a fixed circular orbit for a fixed ω_q decreases as α increases, whereas for a fixed α it increases with increasing ω_q.

Using the spin precession frequency, we differentiated black holes from naked singularities. The range of the angular velocity of a stationary observer can be parametrized by k. For $k = 0.5$, the observer is called a ZAMO. If the precession frequency of test gyroscopes attached to stationary observers moving along two different directions diverge as the observers approach the central object, then the spacetime is a black hole. If the precession frequency along most of the directions remains finite, then the spacetime is a naked singularity. This is

because for black holes the precession frequency diverges as the observer approaches the horizon along all directions, while for naked singularities this divergence appears only when the observer reaches the center of the spacetime along $\theta = \pi/2$.

ACKNOWLEDGMENTS

This work is supported in part by the National Natural Science Foundation of China (NNSFC), Grant No. 11375153 (A. W.) and No. 11675145 (A. W.).

[1] A. G. Riess *et al.*, Astron. J. **116**, 1009 (1998).
[2] P. M. Garnavich *et al.*, Astrophys. J. **509**, 74 (1998).
[3] S. Perlmutter *et al.*, Astrophys. J. **517**, 565 (1999).
[4] Y. Wang and P. Mukherjee, Phys. Rev. D **76**, 103533 (2007).
[5] V. V. Kiselev, Classical Quantum Gravity **20**, 1187 (2003).
[6] Z. Shuang-Yong, Phys. Lett. B **660**, 7 (2008).
[7] A. Vikman, Phys. Rev. D **71**, 023515 (2005).
[8] K. Martin and S. Domenico, Phys. Rev. D **74**, 123503 (2006).
[9] Z. K. Guo, Y. S. Piao, X. Zhang, and Y. Z. Zhang, Phys. Lett. B **608**, 177 (2005).
[10] J. Q. Xia, B. Feng, and X. Zhang, Phys. Rev. D **74**, 083521 (2006).
[11] R. Yang and X. Gao, Chin. Phys. Lett. **26**, 089501 (2009).
[12] T. Chiba, Phys. Rev. D **60**, 083508 (1999).
[13] N. A. Bahcall, J. P. Ostriker, S. Perlmutter, and P. J. Steinhardt, Science **284**, 1481 (1999).
[14] P. J. Steinhardt, L. M. Wang, and I. Zlatev, Phys. Rev. D **59**, 123504 (1999).
[15] M. Azreg-Aïnou and M. E. Rodrigues, J. High Energy Phys. 09 (2013) 146.
[16] M. Azreg-Aïnou, Eur. Phys. J. C **75**, 34 (2015).
[17] B. B. Thomas, M. Saleh, and T. C. Kofane, Gen. Relativ. Gravit. **44**, 2181 (2012).
[18] A. Younas, M. Jamil, S. Bahamonde, and S. Hussain, Phys. Rev. D **92**, 084042 (2015).
[19] M. Azreg-Aïnou, S. Bahamonde, and M. Jamil, Eur. Phys. J. C **77**, 414 (2017).
[20] E. T. Newman and A. I. Janis, J. Math. Phys. (N.Y.) **6**, 915 (1965).
[21] M. Azreg-Aïnou, Phys. Rev. D **90**, 064041 (2014).
[22] B. Toshmatov, Z. Stuchlik, and B. Ahmedov, Eur. Phys. J. Plus **132**, 98 (2017).
[23] Z. Xu and J. Wang, Phys. Rev. D **95**, 064015 (2017).
[24] J. Lense and H. Thirring, Phys. Zs. **19**, 33 (1918).
[25] B. Mashhoon, F. W. Hehl, and D. S. Theiss, Gen. Relativ. Gravit. **16**, 711 (1984).
[26] L. I. Schiff, Phys. Rev. Lett. **4**, 215 (1960).
[27] W. de Sitter, Mon. Not. R. Astron. Soc. **77**, 155 (1916).
[28] W. Rindler, *Relativity: Special, General, and Cosmological* (Oxford University, New York, 2006).
[29] C. W. F. Everitt *et al.*, Phys. Rev. Lett. **106**, 221101 (2011).
[30] K. I. Sakina and J. Chiba, Phys. Rev. D **19**, 2280 (1979).
[31] J. B. Hartle, *Gravity: An Introduction to Einstein's General Relativity* (Pearson, San Francisco, 2003).
[32] J. H. Chen and Y. J. Wang, Chin. Phys. Lett. **24**, 3063 (2007).
[33] C. Chakraborty and P. Majumdar, Classical Quantum Gravity **31**, 075006 (2014).
[34] C. Chakraborty, P. Kocherlakota, M. Patil, S. Bhattacharyya, P. S. Joshi, and A. Krloak, Phys. Rev. D **95**, 084024 (2017).
[35] C. Chakraborty, P. Kocherlakota, and P. S. Joshi, Phys. Rev. D **95**, 044006 (2017).
[36] N. Straumann, *General Relativity with Applications to Astrophysics* (Springer, New York, 2009).
[37] J. M. Bardeen, Astrophys. J. **162**, 71 (1970).
[38] C. W. Misner, K. S. Thorne, and J. A. Wheeler, *Gravitation* (Freeman, San Francisco, 1973).